



## Article

# Detection of Polystyrene Microplastic Particles in Water Using Surface-Functionalized Terahertz Microfluidic Metamaterials

Sae June Park <sup>1</sup>  and Yeong Hwan Ahn <sup>2,\*</sup> 

<sup>1</sup> School of Electronic Engineering and Computer Science, Queen Mary University of London, London E1 4NS, UK; s.j.park@qmul.ac.uk

<sup>2</sup> Department of Physics and Department of Energy Systems Research, Ajou University, Suwon 16499, Korea

\* Correspondence: ahny@ajou.ac.kr

**Abstract:** We propose a novel method for detecting microplastic particles in water using terahertz metamaterials. Fluidic channels are employed to flow the water, containing polystyrene spheres, on the surface of the metamaterials. Polystyrene spheres are captured only near the gap structure of the metamaterials as the gap areas are functionalized. The resonant frequency of terahertz metamaterials increased while we circulated the microplastic solution, as polystyrene spheres in the solution are attached to the metamaterial gap areas, which saturates at a specific frequency as the gap areas are filled by the polystyrene spheres. Experimental results were revisited and supported by finite-difference time-domain simulations. We investigated how this method can be used for the detection of microplastics with various solution densities. The saturation time of the resonant frequency shift was found to decrease, while the saturated resonant frequency shift increased as the solution density increased.

**Keywords:** terahertz spectroscopy; metamaterials; sensors; microplastics; lab-on-a-chip



**Citation:** Park, S.J.; Ahn, Y.H.

Detection of Polystyrene Microplastic Particles in Water Using Surface-Functionalized Terahertz Microfluidic Metamaterials. *Appl. Sci.* **2022**, *12*, 7102. <https://doi.org/10.3390/app12147102>

Academic Editors: Matt Oehlschlaeger and Mona M. Hella

Received: 11 June 2022

Accepted: 12 July 2022

Published: 14 July 2022

**Publisher's Note:** MDPI stays neutral with regard to jurisdictional claims in published maps and institutional affiliations.



**Copyright:** © 2022 by the authors. Licensee MDPI, Basel, Switzerland. This article is an open access article distributed under the terms and conditions of the Creative Commons Attribution (CC BY) license (<https://creativecommons.org/licenses/by/4.0/>).

## 1. Introduction

Microplastics are defined as plastic particles with a size between 1  $\mu\text{m}$  and 5 mm, which have become a tremendous issue for the aquatic environment [1,2], and subsequently may affect human health through the food chain [2]. For example, microbeads composed of either polyethylene, polypropylene, or polystyrene have been used in various hygiene products such as toothpaste, shampoo, conditioner, and body wash and have been found to be accumulated in seafood, oceans, freshwater lakes, and rivers [3–6]. It was reported that the typical size of microbeads detected in bottled water is between 1 and 5  $\mu\text{m}$  [7]. Various methods including Fourier transform infrared spectroscopy (FTIR), and Raman spectroscopy have been employed to both qualitatively and quantitatively monitor microplastics in aquatic environments [8–10]. However, their limitations in measurement time, target particle size, and complex pre-treatment steps (e.g., density separation) make developing novel in-situ detection methods for microplastics in water environments imperative [2].

Metamaterials are artificially designed structures that interact with electromagnetic waves at a specific frequency, determined by their geometrical parameters and surrounding dielectric environment [11–13]. The inductive–capacitive (LC) resonance mode in metamaterials, described by  $f_0 = 1/2\pi\sqrt{LC}$ , where  $L$  is the inductance and  $C$  is the capacitance of the gap area, has been extensively investigated in biosensing research owing to its controllability and high sensitivity [14–22]. It is noteworthy that it has been demonstrated that metamaterials operating in the terahertz (THz) frequency range offer ideal platforms for dielectric sensing, more specifically for sensing a few micron-sized target materials such as fungi, and bacteria in ambient and aqueous environments [23–26]. Additionally, the sensitivity of THz metamaterials as a function of the relative position of the polystyrene microbead has been recently studied explicitly [27].

Therefore, it is pertinent to exploit THz metamaterials to develop novel microplastic sensors working in water environments. As the detection volume of THz metamaterials is strongly confined to the region near the surface of the metamaterials [15,28], a fluidic channel with a thin water layer can be integrated into the metamaterials to minimize the THz absorption from water and flow the microplastic solution on the surface of the metamaterials [29–36]. Further to this, the gap area of the metamaterials could be functionalized to capture the microplastics only near the gap structure of the metamaterials where the actual detection occurs [27]. However, the in situ detection of microplastics using functionalized THz metamaterials devices in water environments has not been demonstrated yet.

Here, we investigated a new approach to detecting microplastics in aqueous environments using surface-functionalized THz microfluidic metamaterials that can overcome the limitation of existing methods based on FTIR and Raman spectroscopy. The fast circulation technique has been employed to enhance the detection speed and sensitivity for sensing microplastics in aqueous environments. We monitored the change in the resonant frequency of the metamaterials with in situ THz spectroscopy while circulating the microplastic solution on the surface-functionalized metamaterials using fluidic channel devices. Finite-difference time-domain (FDTD) simulations were performed to understand the experimental results. Additionally, we studied the saturation behavior in the resonant frequency shift as polystyrene-microplastic spheres (PS) were attached to the gap area of the metamaterials for various PS solution densities.

## 2. Results and Discussions

Fluidic channel devices that incorporate the functionalized metamaterials were fabricated as shown schematically in Figure 1a,b. The key idea is that the gap areas of metamaterials are filled by the target materials while the PS solution is continuously circulated as the gap area are functionalized. We note that plasmonic and metamaterial sensors generally address the density of target material at the sensor surface [16,23,37], while it is the volume density that is required for sensing in the aqueous environment. We monitored the change in the resonant frequency of the metamaterials with in situ THz spectroscopy while injecting the PS solution into the fluidic device. The transmission amplitudes of THz metamaterial devices were obtained from a conventional in situ THz time-domain spectroscopy system with an acquisition time of 4 s as described elsewhere [38,39].

A conventional photolithography method was used to pattern metamaterials on a high-resistivity Si substrate with a thickness of 550  $\mu\text{m}$ . Cr/Au (2 nm/98 nm) metal layers were deposited to define the arrays of the split-ring resonator (SRR) with a periodicity of 50  $\mu\text{m}$ . The SRR consists of a rectangle ring with outer dimensions of  $36 \times 36 \mu\text{m}^2$ , a gap width of 3  $\mu\text{m}$  and a gap length of 10  $\mu\text{m}$ . The linewidth and the thickness of the SRR were chosen to be 4  $\mu\text{m}$  and 100 nm, respectively. The geometrical parameters of the metamaterial unit cell are shown in Figure 1c. Metamaterials were then functionalized to capture the PS in the water by partially coating an adhesive poly-L-lysine (PLL) layer only in the gap area, while the rest of the area was coated with an anti-adhesive hexamethyldisilazane (HMDS) layer [27]. The full-width at half maximum of the metapattern resonance in water was 130 GHz and we obtained the resonant peak position by using the Gaussian fitting with an uncertainty of around 1 GHz. To circulate the PS solution on the metasurface, we fabricated the polydimethylsiloxane (PDMS) fluidic channel with a height of 20  $\mu\text{m}$  and a width of 2 mm on the metamaterials. The height of the PDMS channel is determined by the height of the SU-8 mold which was used to fabricate the PDMS channel. The PDMS fluidic channel was bonded to the surrounding substrate area of the metasurface using the plasma surface treatment method [31]. We note that the PS solution was circulated through the fluidic channel using a peristaltic pump with an 80  $\mu\text{L}/\text{min}$  rate.

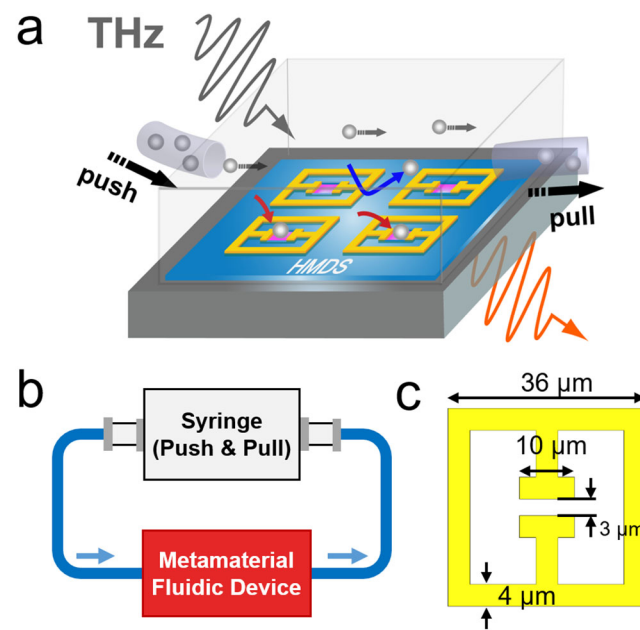


**Figure 1.** (a) Schematic of surface-functionalized fluidic THz metamaterials for microplastic detection in the aqueous environment. The gap area is coated by adhesive polymer (pink area), whereas it is coated by HMDS (blue area), which repels the microplastics. (b) Schematic for the experiments in which the fluidic metamaterials device is connected to a peristaltic pump for the fast circulation of the analyte solution. (c) SRR pattern design used in this work.

Figure 2a shows the separated THz transmission amplitudes of the surface-functionalized microfluidic metamaterials when the water (black solid line) and PS solution (red solid line) was circulated through the fluidic channel. The inset of Figure 2a shows an optical image of fabricated metamaterials after the circulation of PS solution through the fluidic channel. The polarization direction of the incident THz waves is indicated with a white arrow. It was clearly shown that the PSs were captured only in the functionalized gap areas where the PLL layer was deposited, while HMDS-coated area repelled the PS in the water [27]. We observed a 15.4 GHz blue-shift in the resonant frequency from 717 to 732 GHz with the presence of the PS in the water. We note that the blue-shift occurred as the PS in the water decreased the effective dielectric constant of the target solution due to its low dielectric constant ( $\epsilon_{PS} = 2.56$ ) [27] when compared to that of water ( $\epsilon_{water} = 4.8$ ) [31]. At the low density regime, the blue-shift induced by the presence of the PS in the water can be quantified by the following relationship:  $\Delta f/f_0 = -\alpha N_{PS}(\epsilon_{PS} - \epsilon_{water})/\epsilon_{eff}$ , where  $\alpha$  is a sensitivity coefficient,  $N_{PS}$  is the average number of PS in the gap areas, and  $\epsilon_{eff}$  is the effective dielectric constant near the gap area, which is determined by the combined contributions of the dielectric constants of the substrate and the water [23].  $\epsilon_{eff}$  can be obtained from the relation of  $f_{water} = f_{air}/(\epsilon_{eff})^{1/2}$ , where  $f_{water}$  is the resonant frequency of the metamaterials with an overlaid water layer on the substrate and  $f_{air}$  is the resonant frequency of the metamaterials without the substrate (air embedded). We also note that the fluidic channel device without metamaterials pattern was used as a reference to mitigate the transmission loss from the water layer.

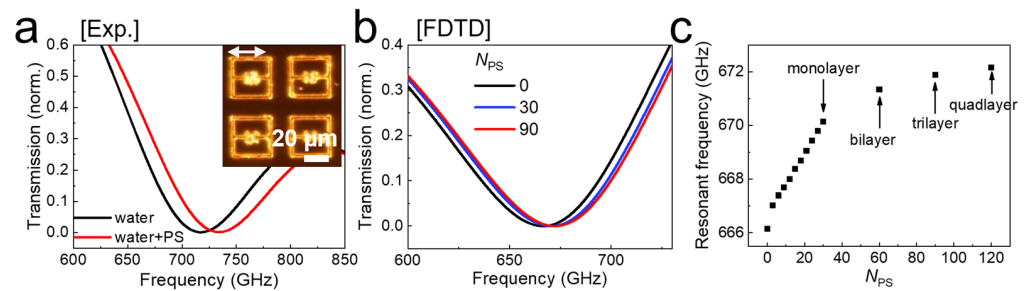


**Figure 2.** (a) Experimentally obtained THz transmission amplitude (normalized) of the surface-functionalized fluidic metamaterials after circulation of the specimen with (red solid line) and without (black solid line) the PS in the water. (inset) Dark-field microscope image of metamaterials with PS captured in the gap area. (b) Simulated THz transmission amplitude of the metamaterials with a 20  $\mu\text{m}$  thick water layer for  $N_{PS} = 0, 30, 90$ . (c) The resonant frequency of the metamaterials as a function of  $N_{PS}$ .

To verify and understand our experimental findings, we performed FDTD simulations using commercial software (CST Studio Suite 2022). The time-domain solver was used to minimize the effect of the internal reflection from the substrate. The geometric parameters and periodic boundary conditions were adopted from the metamaterials used in the experiments. Dielectric constants of 11.8, 4.8, and 2.56, were used for silicon, water, and PS structures, respectively. Two-ports were assigned to the simulation model to generate and receive a linearly polarized incident THz plane wave in the time-domain. We then performed a fast-Fourier transform to obtain the frequency-domain transmission amplitude of the metamaterials. Figure 2b shows the simulated transmission amplitudes of the metamaterials with a 20  $\mu\text{m}$  thick water layer for  $N_{PS} = 0, 30, 90$ . The resonant frequency of 667 GHz was observed for  $N_{PS} = 0$  and the blue-shift of the resonant frequency occurred as  $N_{PS}$  increased. A discrepancy between the experimental results and simulations in the resonant frequency of the metamaterials was observed, which can be attributed to the fabrication tolerance in the experiments. We note that  $N_{PS}$  was first gradually increased to  $N_{PS} = 30$  with a step of three until there was no space to locate additional PS in the gap area, then we increased  $N_{PS}$  with a step of 30 up to  $N_{PS} = 120$  by adding the additional PS layer that consists of 30 PS right above the existing PS layer. The resonant frequency of the metamaterials as a function of  $N_{PS}$  was investigated in Figure 2c to see how the presence of the PS in the water layer affects the resonant frequency shift behavior. The amount of blue-shift increased as the number of PS layers increased, but was saturated at a specific frequency owing to the confined effective sensing volume of the metamaterials near the gap area; this is consistent with the saturation thickness of 1.5  $\mu\text{m}$  estimated for the gap-width of 3  $\mu\text{m}$  [28]. Conversely, in the monolayer case (for  $N_{PS} < 30$ ), the sensitivity coefficient  $\alpha$  of  $7.1 \times 10^{-4}$  was obtained, when  $f_{air} = 1963$  GHz and  $\epsilon_{eff} = 8.66$ .

In order to study the resonant frequency shift behavior of the surface functionalized fluidic metamaterials, we performed in situ THz spectroscopy while we were circulating the PS solution with a density of  $2 \times 10^8$   $\text{mL}^{-1}$  through the fluidic channel. Figure 3a shows THz transmission amplitude as a function of the circulation time of the PS solution. The blue-shift behavior was observed as the PLL layer in the gap area attracted the PS in the solution. In Figure 3b, we extracted the resonant frequency from Figure 3a as a function of circulation time. We note that a fluctuation was observed in the extracted resonant frequency over circulation time that could be attributed to the mechanical motion of the peristaltic pump [40,41]. Therefore, the fitted curve of the resonant frequency (red line) was plotted along with the extracted resonant frequency (black square dots). The resonant frequency of the metamaterials increased while the PSs in the solution were being attached to the gap area but was saturated at a specific frequency as there is no change in the effective dielectric constant of the gap area after a certain level of accumulation of the PS in the gap area over time, as indicated from our simulation results in Figure 2c.

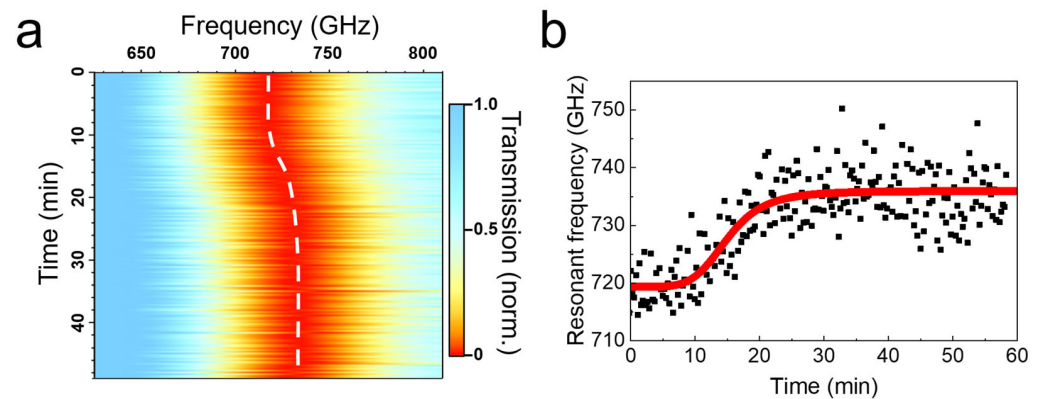


**Figure 3.** (a) A color-scale plot of the normalized transmission amplitude as a function of circulation time of the PS solution. (b) The extracted (black dots) resonant frequency as a function of the circulation time. Red line indicates the fitted curve to the experimental data.

To investigate the effect of the PS solution density on the saturation behavior of the resonance, we performed the same in situ THz spectroscopy again but for various PS solution densities ( $2 \times 10^8$ ,  $1 \times 10^9$ ,  $3 \times 10^9$ ,  $6 \times 10^9$  mL<sup>-1</sup>). In Figure 4, the saturation time ( $T_{sat}$ ) of the resonant frequency shift and the saturated resonant frequency ( $\Delta f_{max}$ ) were plotted as a function of the PS solution density. Here,  $T_{sat}$  corresponds to the time when the resonant frequency shift reaches the half of the maximum frequency shift.  $\Delta f$ -time curves for different solution densities were best fitted with the sigmodal function of  $\Delta f = \Delta f_{max} (1 - 1 / (1 + (t / T_{sat})^p))$ , where  $p$  is the exponent. The saturation time of 16.6 min was obtained with the PS solution density of  $2 \times 10^8$  mL<sup>-1</sup>, which decreased to 18.5 s with the PS solution density of  $6 \times 10^9$  mL<sup>-1</sup>. We note that FTIR and Raman spectroscopy have been often employed to detect microplastics in water [8–10]. However, a liquid sample containing microplastics must go through a pre-treatment step called density separation. The density separation extracts microplastics from the sample liquid by either letting microplastics float or sink in solutions with higher or lower densities than the microplastics [8–10]. This process makes the detection techniques employing FTIR and Raman spectroscopy a time-consuming job, which often takes 5 h to up to 1 day [8]. On the other hand, we could detect microplastics in water with in situ THz spectroscopy by using surface-functionalized fluidic metamaterials. The saturated resonant frequency shift increased further from 15 to 24 GHz as we increased the PS solution density from  $2 \times 10^8$  to  $6 \times 10^9$  mL<sup>-1</sup> even though it was expected that the number of the accumulated PS in the gap area would be similar for different PS solution densities. This could be explained by the fact that the effective dielectric constant of the surrounding PS solution also decreases as the PS solution density increases, owing to the low dielectric constant of the PS compared to the water, leading to a further increase in the saturated resonant frequency shift. It is noteworthy that we reported the relationship between the dielectric constant of overlaid liquid and the resonant frequency shift in our previous study [31]. For instance, we estimated the effective dielectric constant for the  $6 \times 10^9$  mL<sup>-1</sup> case from the saturated frequency shift and found that the dielectric constant decreased by  $-1.0$  when compared to the water case.



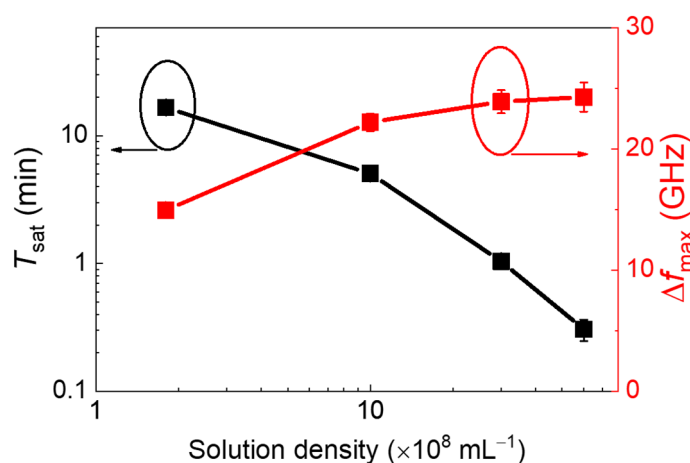


**Figure 4.** Saturation time of the resonant frequency shift (black square dots), and saturated resonant frequency shift (red square dots) as a function of the PS solution density. Error bars indicate the standard deviation extracted from the fitting process.

### 3. Conclusions

We investigated a novel real-time microplastic sensor in a water environment by performing in situ THz spectroscopy on surface-functionalized fluidic metamaterials. PSs were only captured in the gap structure of the metamaterials as the PLL layer in the gap attracted the PS in the water, while HMDS coated area repelled the PS. We showed that the resonant frequency of metamaterials increased as the PSs were captured in the gap area. Also, we monitored the resonant frequency change while we were circulating the PS solution through the fluidic channel and extracted the saturation time of the resonant frequency shift, and the saturated resonant frequency shift for various PS solution densities. Experimental results were confirmed and supported by FDTD simulation results. We successfully demonstrated the detection of the PS in water with in situ THz spectroscopy by using surface-functionalized fluidic metamaterials. We anticipate that this work will contribute to the development of real-time, on-site, cost-efficient, and highly sensitive microplastic sensors to tackle the absence of efficient microplastic sensors working in an aqueous environment.

**Author Contributions:** Conceptualization, Y.H.A.; Data curation, S.J.P.; Formal analysis, S.J.P.; Funding acquisition, Y.H.A.; Investigation, S.J.P. and Y.H.A.; Methodology, Y.H.A.; Writing—original draft, S.J.P. and Y.H.A. All authors have read and agreed to the published version of the manuscript.

**Funding:** This work was supported by the Midcareer Researcher Program (2020R1A2C1005735) and Basic Science Research Program (2021R1A6A1A10044950) through a National Research Foundation grant funded by the Korea Government.

**Data Availability Statement:** Not applicable.

**Conflicts of Interest:** The authors declare no conflict of interest.

### References

- Dehaut, A.; Cassone, A.L.; Frère, L.; Hermabessiere, L.; Himber, C.; Rinnert, E.; Rivière, G.; Lambert, C.; Soudant, P.; Huvet, A.; et al. Microplastics in seafood: Benchmark protocol for their extraction and characterization. *Environ. Pollut.* **2016**, *215*, 223–233. [[CrossRef](#)] [[PubMed](#)]
- Lv, L.; He, L.; Jiang, S.; Chen, J.; Zhou, C.; Qu, J.; Lu, Y.; Hong, P.; Sun, S.; Li, C. In situ surface-enhanced Raman spectroscopy for detecting microplastics and nanoplastics in aquatic environments. *Sci. Total Environ.* **2020**, *728*, 138449. [[CrossRef](#)]
- Lam, C.S.; Ramanathan, S.; Carbery, M.; Gray, K.; Vanka, K.S.; Maurin, C.; Bush, R.; Palanisami, T. A Comprehensive Analysis of Plastics and Microplastic Legislation Worldwide. *Water Air Soil Pollut.* **2018**, *229*, 345. [[CrossRef](#)]
- McDevitt, J.P.; Criddle, C.S.; Morse, M.; Hale, R.C.; Bott, C.B.; Rochman, C.M. Addressing the Issue of Microplastics in the Wake of the Microbead-Free Waters Act—A New Standard Can Facilitate Improved Policy. *Environ. Sci. Technol.* **2017**, *51*, 6611–6617. [[CrossRef](#)] [[PubMed](#)]

5. Rochman, C.M.; Brookson, C.; Bikker, J.; Djuric, N.; Earn, A.; Bucci, K.; Athey, S.; Huntington, A.; McIlwraith, H.; Munno, K.; et al. Rethinking microplastics as a diverse contaminant suite. *Environ. Toxicol. Chem.* **2019**, *38*, 703–711. [[CrossRef](#)]
6. Santillo, D.; Miller, K.; Johnston, P. Microplastics as contaminants in commercially important seafood species. *Integr. Environ. Assess. Manag.* **2017**, *13*, 516–521. [[CrossRef](#)] [[PubMed](#)]
7. Li, Y.; Li, W.; Jarvis, P.; Zhou, W.; Zhang, J.; Chen, J.; Tan, Q.; Tian, Y. Occurrence, removal and potential threats associated with microplastics in drinking water sources. *J. Environ. Chem. Eng.* **2020**, *8*, 104527. [[CrossRef](#)]
8. Huppertsberg, S.; Knepper, T.P. Instrumental analysis of microplastics—Benefits and challenges. *Anal. Bioanal. Chem.* **2018**, *410*, 6343–6352. [[CrossRef](#)]
9. Mani, T.; Blarer, P.; Storck, F.R.; Pittroff, M.; Wernicke, T.; Burkhardt-Holm, P. Repeated detection of polystyrene microbeads in the lower Rhine River. *Environ. Pollut.* **2019**, *245*, 634–641. [[CrossRef](#)]
10. Prata, J.C.; da Costa, J.P.; Duarte, A.C.; Rocha-Santos, T. Methods for sampling and detection of microplastics in water and sediment: A critical review. *Trends Anal. Chem.* **2019**, *110*, 150–159. [[CrossRef](#)]
11. Chen, H.T.; O'Hara, J.F.; Azad, A.K.; Taylor, A.J.; Averitt, R.D.; Shrekenhamer, D.B.; Padilla, W.J. Experimental demonstration of frequency-agile terahertz metamaterials. *Nat. Photonics* **2008**, *2*, 295–298. [[CrossRef](#)]
12. Chen, H.T.; Padilla, W.J.; Zide, J.M.O.; Gossard, A.C.; Taylor, A.J.; Averitt, R.D. Active terahertz metamaterial devices. *Nature* **2006**, *444*, 597–600. [[CrossRef](#)] [[PubMed](#)]
13. Smith, D.R.; Pendry, J.B.; Wiltshire, M.C.K. Metamaterials and negative refractive index. *Science* **2004**, *305*, 788–792. [[CrossRef](#)] [[PubMed](#)]
14. Meng, K.; Park, S.J.; Burnett, A.D.; Gill, T.; Wood, C.D.; Rosamond, M.; Li, L.H.; Chen, L.; Bacon, D.R.; Freeman, J.R.; et al. Increasing the sensitivity of terahertz split ring resonator metamaterials for dielectric sensing by localized substrate etching. *Opt. Express* **2019**, *27*, 23164–23172. [[CrossRef](#)] [[PubMed](#)]
15. O'Hara, J.F.; Singh, R.; Brener, I.; Smirnova, E.; Han, J.; Taylor, A.J.; Zhang, W. Thin-film sensing with planar terahertz metamaterials: Sensitivity and limitations. *Opt. Express* **2008**, *16*, 1786–1795. [[CrossRef](#)]
16. Park, S.J.; Cha, S.H.; Shin, G.A.; Ahn, Y.H. Sensing viruses using terahertz nano-gap metamaterials. *Biomed. Opt. Express* **2017**, *8*, 3551–3558. [[CrossRef](#)]
17. Lee, D.-K.; Kang, J.-H.; Kwon, J.; Lee, J.-S.; Lee, S.; Woo, D.H.; Kim, J.H.; Song, C.-S.; Park, Q.H.; Seo, M. Nano metamaterials for ultrasensitive Terahertz biosensing. *Sci. Rep.* **2017**, *7*, 8146. [[CrossRef](#)]
18. Weisenstein, C.; Schaar, D.; Katharina Wigger, A.; Schäfer-Eberwein, H.; Bossert, A.K.; Haring Bolívar, P. Ultrasensitive THz biosensor for PCR-free cDNA detection based on frequency selective surfaces. *Biomed. Opt. Express* **2020**, *11*, 448–460. [[CrossRef](#)]
19. Zhang, J.; Mu, N.; Liu, L.; Xie, J.; Feng, H.; Yao, J.; Chen, T.; Zhu, W. Highly sensitive detection of malignant glioma cells using metamaterial-inspired THz biosensor based on electromagnetically induced transparency. *Biosens. Bioelectron.* **2021**, *185*, 113241. [[CrossRef](#)]
20. Zhou, J.; Zhao, X.; Huang, G.; Yang, X.; Zhang, Y.; Zhan, X.; Tian, H.; Xiong, Y.; Wang, Y.; Fu, W. Molecule-Specific Terahertz Biosensors Based on an Aptamer Hydrogel-Functionalized Metamaterial for Sensitive Assays in Aqueous Environments. *ACS Sens.* **2021**, *6*, 1884–1890. [[CrossRef](#)]
21. Wang, G.; Zhu, F.; Lang, T.; Liu, J.; Hong, Z.; Qin, J. All-metal terahertz metamaterial biosensor for protein detection. *Nanoscale Res. Lett.* **2021**, *16*, 109. [[CrossRef](#)] [[PubMed](#)]
22. Hou, X.; Chen, X.; Li, T.; Li, Y.; Tian, Z.; Wang, M. Highly sensitive terahertz metamaterial biosensor for bovine serum albumin (BSA) detection. *Opt. Mater. Express* **2021**, *11*, 2268–2277. [[CrossRef](#)]
23. Park, S.J.; Hong, J.T.; Choi, S.J.; Kim, H.S.; Park, W.K.; Han, S.T.; Park, J.Y.; Lee, S.; Kim, D.S.; Ahn, Y.H. Detection of microorganisms using terahertz metamaterials. *Sci. Rep.* **2014**, *4*, 4988. [[CrossRef](#)] [[PubMed](#)]
24. Yang, X.; Yang, K.; Luo, Y.; Fu, W. Terahertz spectroscopy for bacterial detection: Opportunities and challenges. *Appl. Microbiol. Biotechnol.* **2016**, *100*, 5289–5299. [[CrossRef](#)] [[PubMed](#)]
25. Lee, S.H.; Lee, Y.K.; Lee, S.-H.; Kwak, J.; Song, H.S.; Seo, M. Detection and discrimination of SARS-CoV-2 spike protein-derived peptides using THz metamaterials. *Biosens. Bioelectron.* **2022**, *202*, 113981. [[CrossRef](#)]
26. Jun, S.W.; Ahn, Y.H. Terahertz thermal curve analysis for label-free identification of pathogens. *Nat. Commun.* **2022**, *13*, 3470. [[CrossRef](#)]
27. Cha, S.H.; Park, S.J.; Ahn, Y.H. Investigation of sensitivity distribution in thz metamaterials using surface functionalization. *Curr. Opt. Photonics* **2019**, *3*, 566–570. [[CrossRef](#)]
28. Park, S.J.; Yoon, S.A.N.; Ahn, Y.H. Effective sensing volume of terahertz metamaterial with various gap widths. *J. Opt. Soc. Korea* **2016**, *20*, 628–632. [[CrossRef](#)]
29. George, P.A.; Hui, W.; Rana, F.; Hawkins, B.G.; Smith, A.E.; Kirby, B.J. Microfluidic devices for terahertz spectroscopy of biomolecules. *Opt. Express* **2008**, *16*, 1577–1582. [[CrossRef](#)]
30. Astley, V.; Reichel, K.S.; Jones, J.; Mendis, R.; Mittleman, D.M. Terahertz multichannel microfluidic sensor based on parallel-plate waveguide resonant cavities. *Appl. Phys. Lett.* **2012**, *100*, 231108. [[CrossRef](#)]
31. Park, S.J.; Yoon, S.A.N.; Ahn, Y.H. Dielectric constant measurements of thin films and liquids using terahertz metamaterials. *RSC Adv.* **2016**, *6*, 69381–69386. [[CrossRef](#)]
32. Tang, Q.; Liang, M.; Lu, Y.; Wong, P.K.; Wilkink, G.J.; Zhang, D.; Xin, H. Microfluidic Devices for Terahertz Spectroscopy of Live Cells Toward Lab-on-a-Chip Applications. *Sensors* **2016**, *16*, 476. [[CrossRef](#)]

33. Geng, Z.; Zhang, X.; Fan, Z.; Lv, X.; Chen, H. A Route to Terahertz Metamaterial Biosensor Integrated with Microfluidics for Liver Cancer Biomarker Testing in Early Stage. *Sci. Rep.* **2017**, *7*, 16378. [[CrossRef](#)] [[PubMed](#)]
34. Serita, K.; Matsuda, M.; Okada, K.; Murakami, H.; Kawayama, I.; Tonouchi, M. Invited Article: Terahertz microfluidic chips sensitivity-enhanced with a few arrays of meta-atoms. *APL Photonics* **2018**, *3*, 051603. [[CrossRef](#)]
35. Russell, C.; Swithenbank, M.; Wood, C.D.; Burnett, A.D.; Li, L.; Linfield, E.H.; Davies, A.G.; Cunningham, J.E. Integrated On-Chip THz Sensors for Fluidic Systems Fabricated Using Flexible Polyimide Films. *IEEE Trans. Terahertz Sci. Technol.* **2016**, *6*, 619–624. [[CrossRef](#)]
36. Cao, Y.; Nallappan, K.; Guerboukha, H.; Gervais, T.; Skorobogatiy, M. Additive manufacturing of resonant fluidic sensors based on photonic bandgap waveguides for terahertz applications. *Opt. Express* **2019**, *27*, 27663–27681. [[CrossRef](#)]
37. Shih, K.; Pitchappa, P.; Manjappa, M.; Ho, C.P.; Singh, R.; Lee, C. Microfluidic metamaterial sensor: Selective trapping and remote sensing of microparticles. *J. Appl. Phys.* **2017**, *121*, 023102. [[CrossRef](#)]
38. Park, S.J.; Kim, A.R.; Hong, J.T.; Park, J.Y.; Lee, S.; Ahn, Y.H. Crystallization Kinetics of Lead Halide Perovskite Film Monitored by In Situ Terahertz Spectroscopy. *J. Phys. Chem. Lett.* **2017**, *8*, 401–406. [[CrossRef](#)]
39. Kim, H.S.; Ha, N.Y.; Park, J.-Y.; Lee, S.; Kim, D.-S.; Ahn, Y.H. Phonon-Polaritons in Lead Halide Perovskite Film Hybridized with THz Metamaterials. *Nano Lett.* **2020**, *20*, 6690–6696. [[CrossRef](#)]
40. Bromley, A.J.; Holdich, R.G.; Cumming, I.W. Particulate fouling of surface microfilters with slotted and circular pore geometry. *J. Membr. Sci.* **2002**, *196*, 27–37. [[CrossRef](#)]
41. Ma, T.; Sun, S.; Li, B.; Chu, J. Piezoelectric peristaltic micropump integrated on a microfluidic chip. *Sens. Actuator A Phys.* **2019**, *292*, 90–96. [[CrossRef](#)]